

## Article

# Highly Active Large Au Clusters and Even More Active Ag Nanoparticles Supported on Ceria-Zirconia: Impact of Particle Size and Potassium Ion Loading on Activity in Catalytic Transfer Hydrogenation

Ewa M. Iwanek (nee Wilczkowska) <sup>1,\*</sup>, Marek Gliński <sup>1</sup>, Aleksandra Siwiec <sup>1</sup>, Sylwia Siennicka <sup>1</sup>, Magdalena Zybert <sup>1</sup> and Zbigniew Kaszukur <sup>2</sup>

<sup>1</sup> Faculty of Chemistry, Warsaw University of Technology, 00-664 Warsaw, Poland

<sup>2</sup> Institute of Physical Chemistry, Polish Academy of Sciences, 01-224 Warsaw, Poland

\* Correspondence: ewa.iwanek@pw.edu.pl

**Abstract:** Although heterogeneous monometallic gold catalysts are commonly more active when the gold particles are smaller, this study shows that the reverse is true in the case of liquid phase catalytic transfer hydrogenation of acetophenone with 2-pentanol. Higher catalytic activity of larger gold particles, i.e., over 30 nm in diameter, than of smaller particles of average 4 nm in size was observed. Moreover, this effect was contradictory to that observed for supported monometallic silver catalysts in which the interaction with the support and hence particle size was shown to cause drastic changes in the activity in this reaction, with the large particles being completely inactive and tiny ones being the most active system studied. In this reaction, the ceria-zirconia solid solutions were used as the supports for the catalysts and both zirconium doped ceria, as well as cerium doped zirconia carriers were tested. The supports themselves exhibited little activity in this reaction. It was shown that the activity of the supports and catalysts depends on the Ce/Zr ratio and potassium content. Both types of catalysts showed excellent selectivity to 1-phenylethanol and conversion of acetophenone, although it was noted that a high loading of potassium carbonate in the gold catalysts propelled undesired reactions, thereby reducing the selectivity to 1-phenylethanol.

**Keywords:** catalytic transfer hydrogenation; potassium ion doping; ceria-zirconia; large gold particles; silver nanoparticles



**Citation:** Iwanek, E.M.; Gliński, M.; Siwiec, A.; Siennicka, S.; Zybert, M.; Kaszukur, Z. Highly Active Large Au Clusters and Even More Active Ag Nanoparticles Supported on Ceria-Zirconia: Impact of Particle Size and Potassium Ion Loading on Activity in Catalytic Transfer Hydrogenation. *Catalysts* **2022**, *12*, 974. <https://doi.org/10.3390/catal12090974>

Academic Editors: Salvatore Scire` and Leonarda Francesca Liotta

Received: 7 August 2022

Accepted: 29 August 2022

Published: 30 August 2022

**Publisher's Note:** MDPI stays neutral with regard to jurisdictional claims in published maps and institutional affiliations.

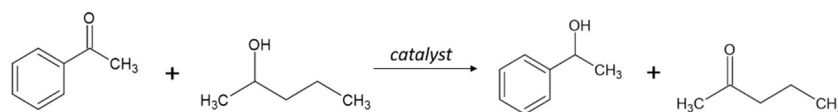


**Copyright:** © 2022 by the authors. Licensee MDPI, Basel, Switzerland. This article is an open access article distributed under the terms and conditions of the Creative Commons Attribution (CC BY) license (<https://creativecommons.org/licenses/by/4.0/>).

## 1. Introduction

Reactions carried out in the presence of heterogeneous catalysts, without the use of toxic solvents, follow the Principles of Green Chemistry and are considered beneficial for the environment [1]. An additional advantage of catalytic transfer hydrogenation is the substitution of gaseous hydrogen with a hydrogen donor, such as an aliphatic alcohol [2–4], which makes the process safer and more cost effective. Heterogeneous gold catalysts have been applied in multiple reactions for decades [5,6], such as vinyl acetate synthesis [7,8], oxidation of carbon monoxide [9–11], hydrochlorination of acetylene [12], combustion of volatile organic compounds (VOCs) [13], oxidation of alcohols [14], water-gas shift reaction [15], hydrogenation [16–19], etc. However, their application in catalytic transfer hydrogenation (CTH) has not been well studied [20]. Moreover, the gold catalysts which have been employed in CTH are usually homogeneous or so-called quasi-homogeneous catalysts [21,22]. Unsupported nanoporous gold has also been shown to be highly selective in similar transfer hydrogenation reactions [23]. Research on the transfer hydrogenation of acetophenone with 2-propanol has shown the influence of the support, namely that the order of activity is Au/TiO<sub>2</sub> > Au/Fe<sub>2</sub>O<sub>3</sub> > Au/C [24]. Despite different conversions of acetophenone, the selectivity was 98–100% for all three types of catalysts. The scheme of the

reaction studied in this paper, namely CTH of acetophenone with 2-pentanol is depicted below (Scheme 1).



**Scheme 1.** Scheme of catalytic hydrogen transfer from 2-pentanol to acetophenone.

Few silver complexes have been used in catalytic transfer hydrogenation [25,26]. Homogeneous silver-containing systems have been reported as catalysts for the hydrogenation of aliphatic and aromatic ketones with gaseous hydrogen [27–29]. However, very few reports pertain to heterogeneous silver catalysts [30]. Among those studied are: Ag/SiO<sub>2</sub> and Ag/TiO<sub>2</sub>. The hydrogenation of crotonaldehyde using these catalysts gave a selectivity to the unsaturated aldehyde below 60%. This suggests that silver catalysts are not as selective as gold catalysts, but no studies comprising analogous synthesis procedures or of both types of catalysts on the same batch of supports have been reported.

Undoped ceria crystallizes in the fluorite-type structure. Zirconium ions can be incorporated into the ceria lattice and cerium ions can be inserted into the Zr nodes of the zirconia lattice. Reports in the literature show that doping ceria with zirconium ions does not affect the symmetry (space group) of the crystal lattice, but changes the lattice parameters [31]. Such a situation occurs at low zirconium loadings, though different papers suggest different scenarios for zirconium loadings of above 25%. At such zirconium contents, there is usually more than one phase present. The stabilization of the tetragonal structure of zirconia by the addition of cerium ions has also been applied in the ceramic industry [32–34], but very few reports of such materials used as catalyst supports can be found [35–38].

Alkali ion promotion and poisoning is a topic which has been of interest in many reactions for decades. Their effect has been investigated on catalysts used in both inorganic and organic reactions, such as: selective catalytic reduction of NO<sub>x</sub> with NH<sub>3</sub> [39], NO decomposition [40,41], synthesis of vinyl acetate [42], ketonization of acetic acid [43], catalytic oxidation of formaldehyde [44], etc. Our previous studies have focused on the effect of potassium ions [45,46] and other alkali metal ions [47] on the activity of gold and silver, as well as bimetallic Au-Ag systems in CO oxidation, C<sub>3</sub>H<sub>8</sub> combustion and NO oxidation. Another study has also shown a decreased reducibility of the catalysts upon doping with alkali metal cations, but the authors found that their presence increased the strength and density of basic sites [48]. Such an effect might be beneficial for catalytic transfer hydrogenation of acetophenone with 2-pentanol and hence doping with potassium ions was used for selected supports and the best performing catalysts.

## 2. Results

There were two types of ceria-zirconia supports applied in this study, namely Ce<sub>1-x</sub>Zr<sub>x</sub>O<sub>2</sub> (x < 0.20) and Zr<sub>1-x</sub>Ce<sub>x</sub>O<sub>2</sub>, where x < 0.10. Selected XRD patterns are shown in Figure 1a. It can be seen that the three Ce<sub>1-x</sub>Zr<sub>x</sub>O<sub>2</sub> supports contained only one phase: the ceria fluorite-type structure (PDF#810792), which is in line with the information available in the literature for zirconium loadings of 25% or lower (PDF#280271). The phase is homogeneous since heterogeneity would result in significantly enlarged eps (microstress parameter, Table 1). The lattice parameter increased along with the decrease in the zirconium content and was 0.5350(1), 0.5362(1) and 0.5374(1) for 20%, 15% and 10% Zr, respectively, which was due to the smaller Zr<sup>4+</sup> ionic radius. The Zr/(Ce + Zr) ratio established with XPS showed a considerable enrichment of the surface of these supports with zirconium (Figure 1b). In fact, it was double the nominal concentration. A thorough investigation in which ceria-zirconia supports were studied by Shah et al. [49], reported a similar finding for such supports used for propane combustion catalysts. Our findings obtained with SEM-EDX, which probed

the supports deeper than XPS and hence the numbers were much closer to the nominal values, which confirmed a surface enrichment of these supports in zirconium.

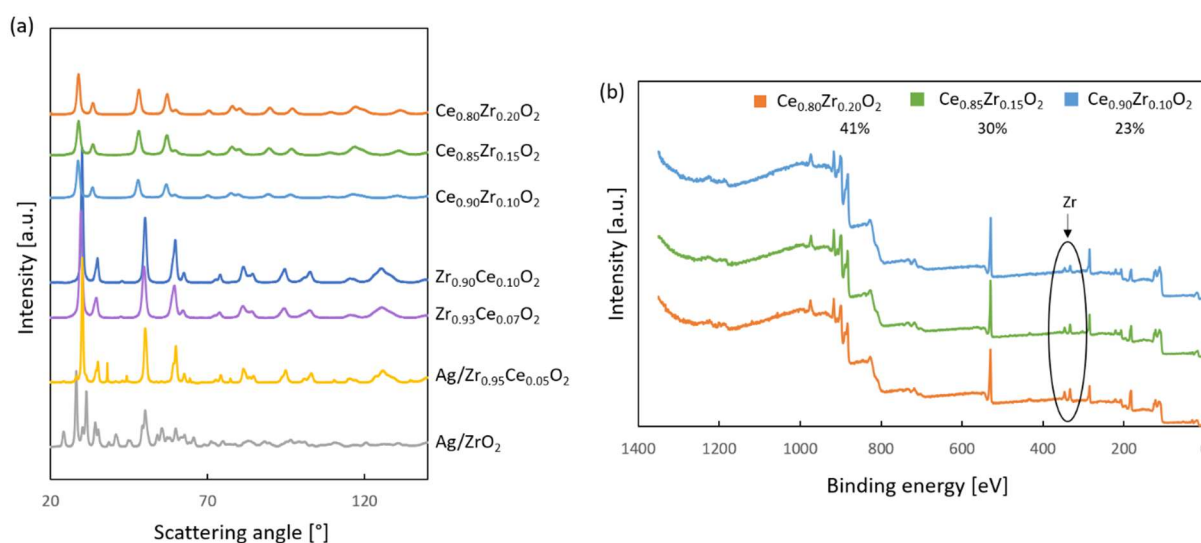


**Figure 1.** Characterization of selected supports and catalysts: (a) diffraction patterns and (b) XPS survey spectra.

**Table 1.** Properties of selected supports.

Sample	Surface Area [m <sup>2</sup> /g]	Particle Size [nm] <sup>1</sup>	Cell Parameter(s) [nm]	Structure; $\epsilon$ <sup>2</sup>
CeO <sub>2</sub>	52.8	6.0(8)	0.5408(2)	cubic; 0.002
Ce <sub>0.90</sub> Zr <sub>0.10</sub> O <sub>2</sub>	95.2	6.5(8)	0.5374(2)	cubic; 0.003
Ce <sub>0.85</sub> Zr <sub>0.15</sub> O <sub>2</sub>	96.0	5.1(8)	0.5362(2)	cubic; 0.002
Ce <sub>0.80</sub> Zr <sub>0.20</sub> O <sub>2</sub>	87.2	5.7(8)	0.5350(2)	cubic; 0.002
ZrO <sub>2</sub>	48.0	10.7(8), 7.1(8)	n.d.	monoclinic, cubic
Zr <sub>0.93</sub> Ce <sub>0.07</sub> O <sub>2</sub>	63.1	7.0(8)	a = 0.364(1), c = 0.523(1)	tetragonal
Zr <sub>0.90</sub> Ce <sub>0.10</sub> O <sub>2</sub>	62.9	7.0(8)	a = 0.363(1), c = 0.523(1)	tetragonal

<sup>1</sup> The particle size was determined from the Williamson–Hall plot (14 reflexes) for zirconium doped ceria and pure ceria (cubic phase), and from the Scherrer equation applied to the (101) reflex for cerium-doped zirconia (tetragonal phase). <sup>2</sup> The values of microstrain parameter,  $\epsilon$ , could be determined only from Williamson–Hall plot that could not be constructed for the tetragonal cerium-doped zirconia due to strong peak overlap and likely size/strain anisotropy.

The doping of ceria with zirconium ions leads to a higher resistance to sintering, which was evidenced by the higher specific surface areas of the Ce<sub>1-x</sub>Zr<sub>x</sub>O<sub>2</sub> samples compared to that of undoped ceria. The values of the areas of the studied zirconium-doped ceria supports fell in the range 87–96 m<sup>2</sup>/g (Table 1), whereas that of the ceria synthesized by the same method, i.e., precipitation using an aqueous ammonia solution, followed by drying and calcination (for details see the Material and Methods) was only 52.8 m<sup>2</sup>/g. The value of the zirconia prepared in an analogous manner was even lower, i.e., 48.0 m<sup>2</sup>/g. The doping of zirconia with cerium ions increased the surface area of the zirconia to 63.0 ± 0.1 m<sup>2</sup>/g. However, in this case, the simultaneous change of the crystal structure should also be taken into account when comparing the supports (Table 1).

The cerium-doped zirconia samples contain only one phase, namely the tetragonal phase with P4<sub>2</sub>/nmc structure (Figure 1a and Table 1), as has been noted for cerium-doped zirconia samples (PDF#381437, PDF#821398 and PDF#800785). The deposition of silver onto

this type of support does not influence the structure of the support. The only difference seen in the diffraction pattern when silver was deposited onto the support, was that one could observe additional peaks, i.e.,  $38.1^\circ$ ,  $44.3^\circ$ ,  $64.5^\circ$  and  $77.5^\circ$  (Supplementary Information: Figure S1), which arose from the presence of metallic silver (PDF#040783). This is different than what was observed by us for the zirconium-doped ceria supports [46], on which the deposition of silver led to well-dispersed silver, which was not visible in the diffraction pattern. Therefore, samples after catalytic transfer hydrogenation were also tested with XRD and size of silver particles calculated for Ag/CZ and Ag/ZC were 9 and 40 nm, respectively, showing a substantial difference in the silver distribution despite the same deposition procedure. This may be due to stronger interaction of silver with the zirconium-doped ceria supports than with the cerium-doped zirconia supports. Alternatively, the character of the interactions may be different. Further studies are needed to determine the exact cause of this difference.

In contrast to the cerium-doped zirconia supports, the obtained zirconia was present in two phases (Figure 1a): monoclinic (PDF#861451) and cubic (PDF#811551). Additionally, peaks from metallic silver (15 nm) were visible in the diffraction pattern. It can therefore be concluded that the incorporation of cerium ions into the zirconia lattice stabilizes the tetragonal structure, which may be beneficial for some applications, perhaps including catalytic activity. In order to verify if there is an effect of the support composition on its activity in catalytic hydrogen transfer from 2-pentanol to acetophenone, all of the supports were tested in this reaction.

Figure 2 depicts the 1-phenylethanol yields obtained on the  $Ce_{1-x}Zr_xO_2$  and  $Zr_{1-x}Ce_xO_2$  supports. It can be seen that the yield of 1-phenylethanol increased with time for all catalyst supports and that the activity of the zirconium-doped ceria samples was substantially higher than that of pure ceria. There was a strong dependence of the yield of 1-phenylethanol on the zirconium loading (Figure 2a). The order of activity was as follows: 10%, 15%, 5%, 20%. This implies that there is an optimum doping of ceria (at about 10% Zr), which allows for the formation of the largest number of active sites. The addition of 5% of Zr was not enough, whereas 15% was already slightly too much and 20% was substantially too much. Despite the trend of the activity of the supports themselves, the support with 15% Zr was used for Au and Ag deposition due to the series of previously performed studies carried out by our group in other reactions [45–47] in order to obtain a greater insight into the same type of catalytic systems.

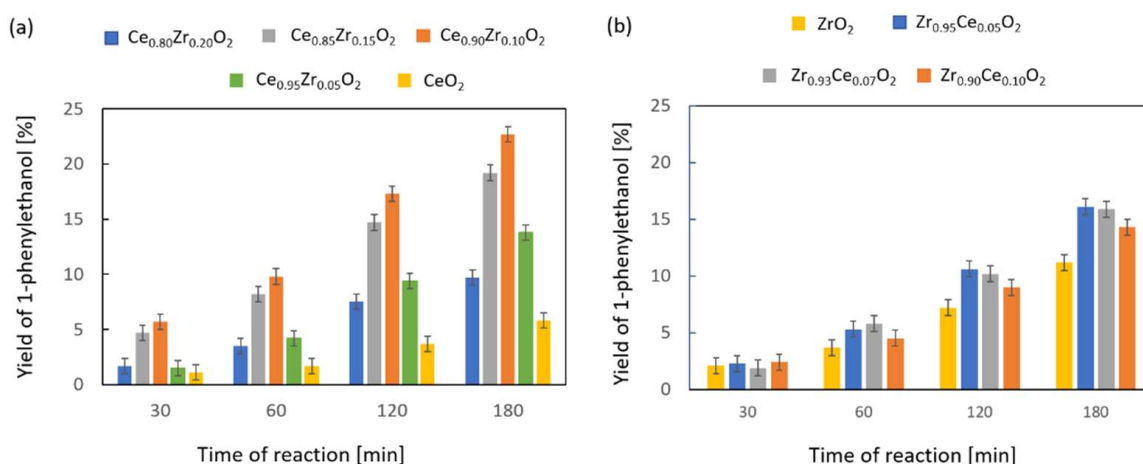


**Figure 2.** Yield of 1-phenylethanol obtained during catalytic transfer hydrogenation of acetophenone with 2-pentanol in the presence of (a)  $Ce_{1-x}Zr_xO_2$  ( $x < 0.2$ ) and (b)  $Zr_{1-x}Ce_xO_2$  ( $x < 0.1$ ).

The activity of pure zirconia was slightly higher than that of pure ceria (Figure 2b), but the cerium-doped zirconia supports exhibited a lower activity than the zirconium-doped ceria supports. In contrast to the zirconium doped ceria samples, the activity of the cerium-

doped zirconia supports showed a much narrower range, and, in fact, was the same at the beginning of the reaction, i.e., 30 min into the reaction, for all studied contents and was very similar after 1 hour of reaction, after which there was a slight diversification of the values. However, it is noteworthy that the topography of the cerium-doped zirconia supports (Figure 3) did not differ much from those of zirconium-doped ceria supports. This is most likely due to the same preparation procedure which included precipitation of the hydroxide, drying and calcining at a final temperature of 550 °C.

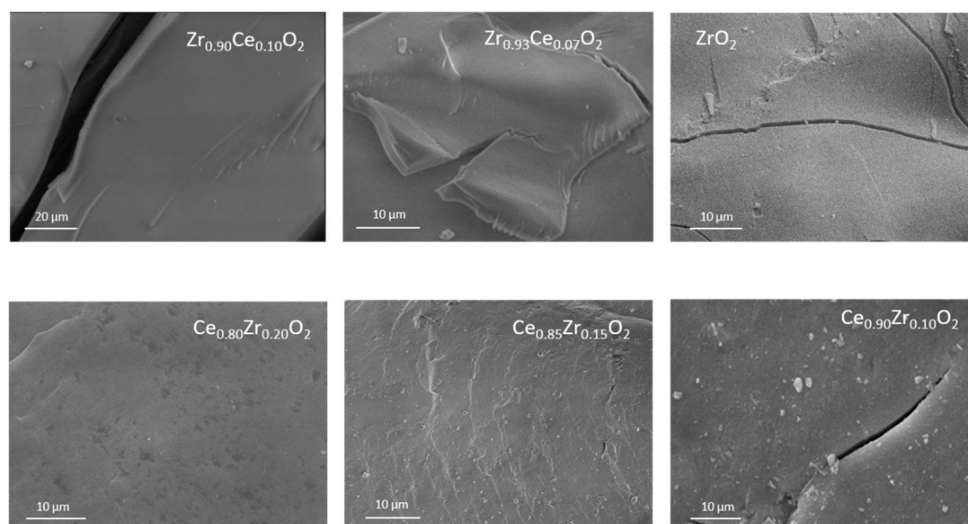


**Figure 3.** SEM images of selected supports.

The results of the activity tests of Au/Ce<sub>0.85</sub>Zr<sub>0.15</sub>O<sub>2</sub> for two different particle sizes are shown in Figure 4a. It is worth noting that the results for this reaction are in sharp contrast with those of other reactions, such as CO oxidation, in which small particles are found to be much more active than larger ones [9,46]. In order to ensure that the difference is not a result of differences in the synthesis, but strictly the particle size, both samples were made from the same batch of Au/Ce<sub>0.85</sub>Zr<sub>0.15</sub>O<sub>2</sub> with the only difference between the samples being the calcination time. The longer calcination time yielded larger gold particles than the shorter calcination time, but the gold loading was the same. In contrast, the opposite was observed for silver (Figure 4b). Both types of catalysts exhibited excellent selectivity (>99%) to 1-phenylethanol. It can be seen that the best Ag catalyst was more active than the best gold catalyst. The reason for the high activity and selectivity is presumed to be the in situ generation of silver nanoparticles. This effect was reported in the case of the catalytic activity of Ag Nps in hydrogenation of ketones with the use of gaseous hydrogen [27], and is consistent with the appearance of a violet color, typical of nano silver particles, during the reaction, as well as the size determined by XRD measurements of the spent sample. The larger Ag particles, obtained through a prolonged sintering time, showed a lower activity than the smaller ones (Figure 4b).

The impact of the potassium ion loading on the activity of Ce<sub>0.85</sub>Zr<sub>0.15</sub>O<sub>2</sub> is shown in Figure 5a. It can be seen that the initial, low concentrations of potassium ions, i.e., 0.3 and 0.6 at% exerted a small, but beneficial effect on the support, whereas the doping of Au/Ce<sub>0.85</sub>Zr<sub>0.15</sub>O<sub>2</sub> (Figure 5b) with those loadings of potassium suppressed the activity of the undoped gold catalyst. This is similar in the case of CO oxidation [45,47]. The further addition of potassium ions had a detrimental effect on the activity of the support and the gold catalyst. It is noteworthy that with potassium ion loadings above 0.6 at%, the yield of 1-phenylethanol observed in the presence of the gold catalyst fell below that of the undoped support. Side and subsequent reactions were responsible for this and the liquid changed from clear and colorless to yellow. The intensity of the color of the solution increased with reaction time, which indicates larger yields of byproducts. In the case of the most active

silver catalyst, the presence of 0.3 at%  $K^+$  caused a decrease in the activity (Figure 5c). Hence, it is possible that in the case of the support, which is much less active, but shows a slight improvement upon doping with potassium ions, there is a different mechanism of the reaction or that the monometallic catalysts have more than one mechanism and the more efficient one is negatively affected by the presence of potassium ions.

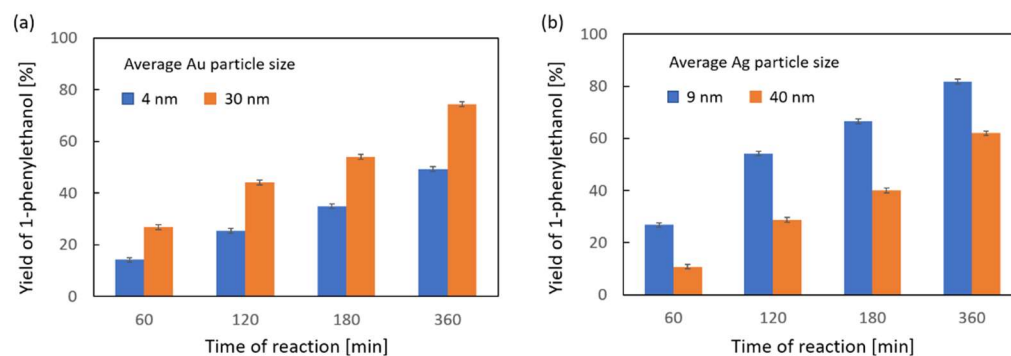


**Figure 4.** Effect of particle size on the yield of 1-phenylethanol obtained during catalytic transfer hydrogenation of acetophenone with 2-pentanol in the presence of (a) Au/Ce<sub>0.85</sub>Zr<sub>0.15</sub>O<sub>2</sub> and (b) Ag/Ce<sub>0.85</sub>Zr<sub>0.15</sub>O<sub>2</sub>.

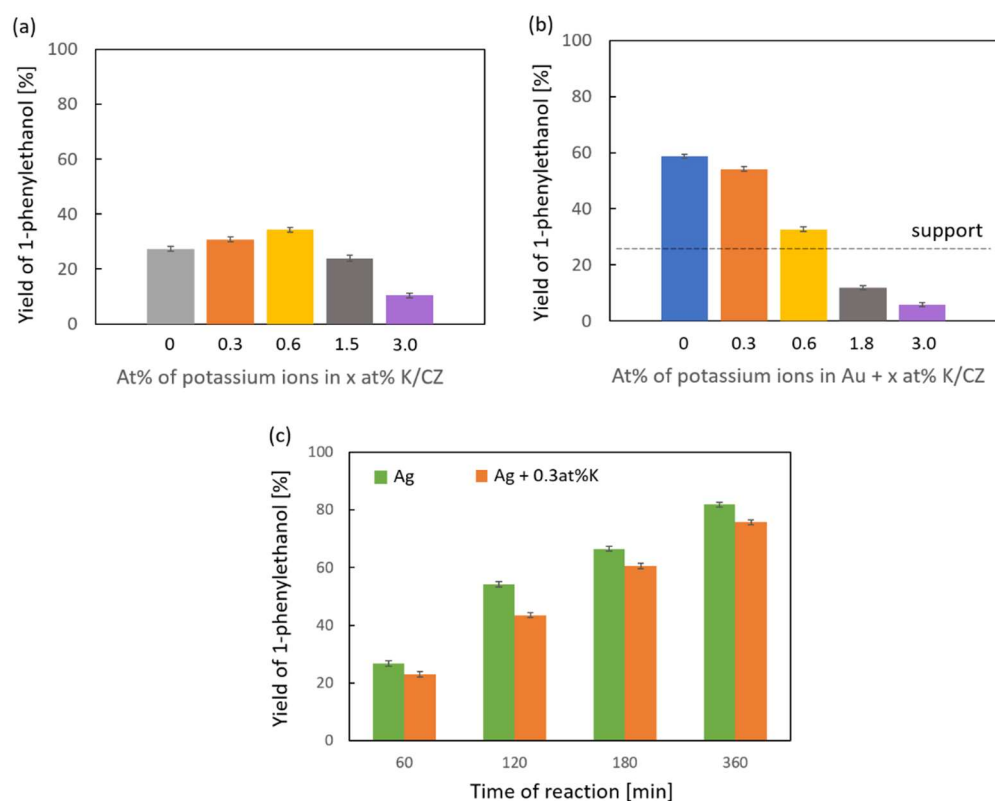


**Figure 5.** Impact of the presence of potassium ions on the yield of 1-phenylethanol after 5 h of reaction over (a) Ce<sub>0.85</sub>Zr<sub>0.15</sub>O<sub>2</sub>, (b) Au/Ce<sub>0.85</sub>Zr<sub>0.15</sub>O<sub>2</sub> and (c) Ag/Ce<sub>0.85</sub>Zr<sub>0.15</sub>O<sub>2</sub>.

A comparison of the results of the activity tests of the supported gold and silver catalysts is presented in Figure 6, in which the number of moles of the desired product is referred to the mass of the active phase (Figure 6a for Au and Figure 6c for Ag) and the different number of moles of the active phase on the surface, due to different particle size (Figure 6b for Au and Figure 6d for Ag). It can be seen that the silver catalysts were much more active per gram of active phase than the gold catalysts (Figure 6a,c). Moreover, a

difference in the conversion in time could be observed, namely, the gold catalysts were the most active during the first hour of reaction, after which the rate of 1-phenylethanol formation decreased. In contrast, the silver catalysts had a similar or higher rate of product formation in the second hour of the catalytic reaction than in the first. When taking into account the particle size (Figure 6b,d), and hence the number of surface moles of the active phase, it can be seen that for the gold catalysts, the difference in the rate of product formation is strongly dependant on the size of the active phase particles, whereas the rate on silver catalysts does not differ as much for the two studied particle sizes.

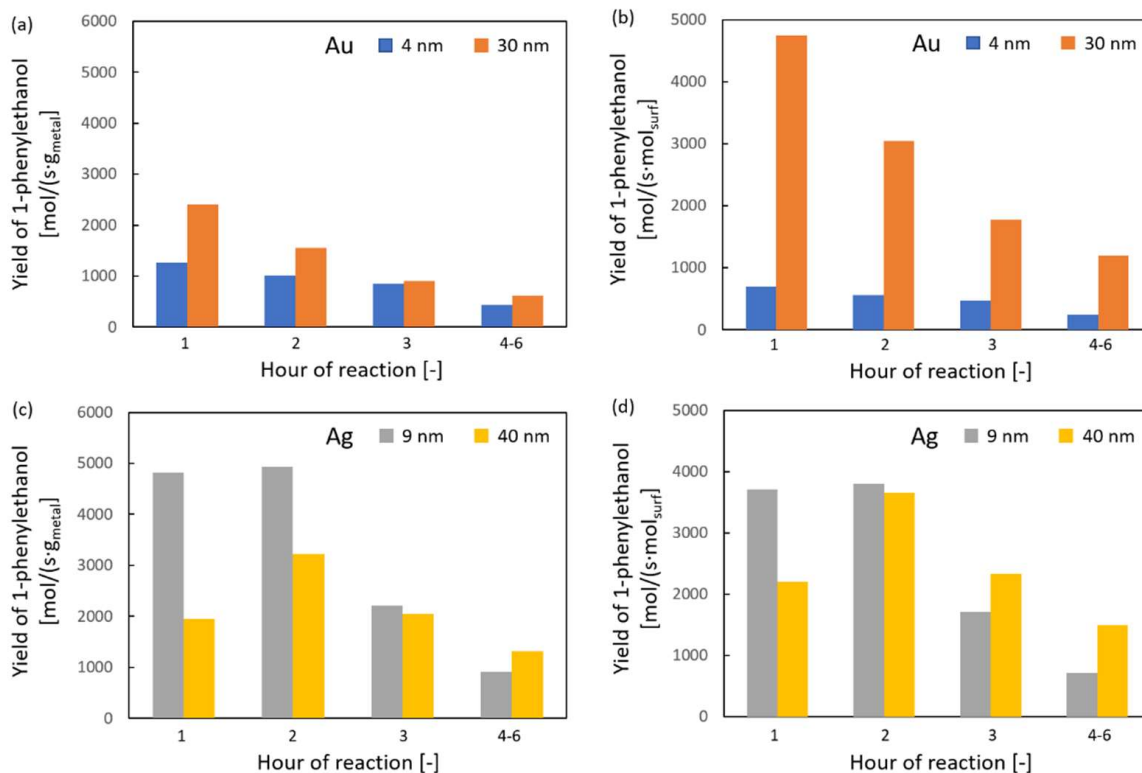


**Figure 6.** Yield of 1-phenylethanol during the course of the reaction referred to the mass of the active phase: (a,c), and to the surface number of moles of the active phase: (b,d).

The gold catalysts supported on cerium-doped zirconia (Figure 7a) showed very little activity in the studied reaction. In fact, it can be seen that the zirconium-doped ceria loaded with 0.6 at%  $K^+$  was more active than the cerium-doped zirconia gold catalysts. The activity of  $Au/Zr_{0.90}Ce_{0.10}O_2$  and  $Au/Zr_{0.93}Ce_{0.07}O_2$  in the studied reaction was comparable. In order to check the distribution of the gold on  $Zr_{0.93}Ce_{0.07}O_2$ , elemental maps were obtained. They are presented in Figure 8. These show a uniform distribution of all the elements, including gold, which, together with the lack of visible gold agglomerates in the SEM images, means that the particles are comparable in size to those which were very active on  $Ce_{0.85}Zr_{0.15}O_2$ . This shows how important the choice of the proper support really is for the monometallic gold catalyst, which is also the case for monometallic silver catalysts (Figure 7b). It is noteworthy that the zirconia supported silver catalyst was less active than the cerium-doped zirconia supported silver catalyst. However, this might be simply a result of the higher surface area due to the incorporation of ceria into the structure (Table 1).

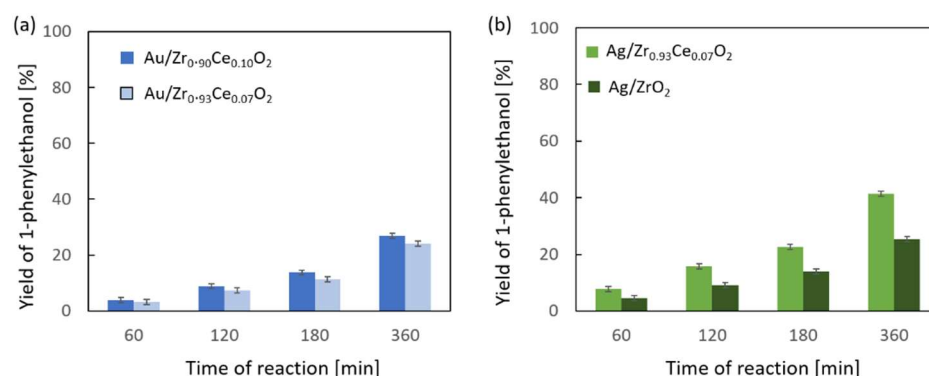


**Figure 7.** Activity test results of catalysts supported on cerium-doped zirconia: yield of 1-phenylethanol obtained during catalytic transfer hydrogenation of acetophenone with 2-pentanol in the presence of (a) Au/ZC and (b) Ag/ZC.

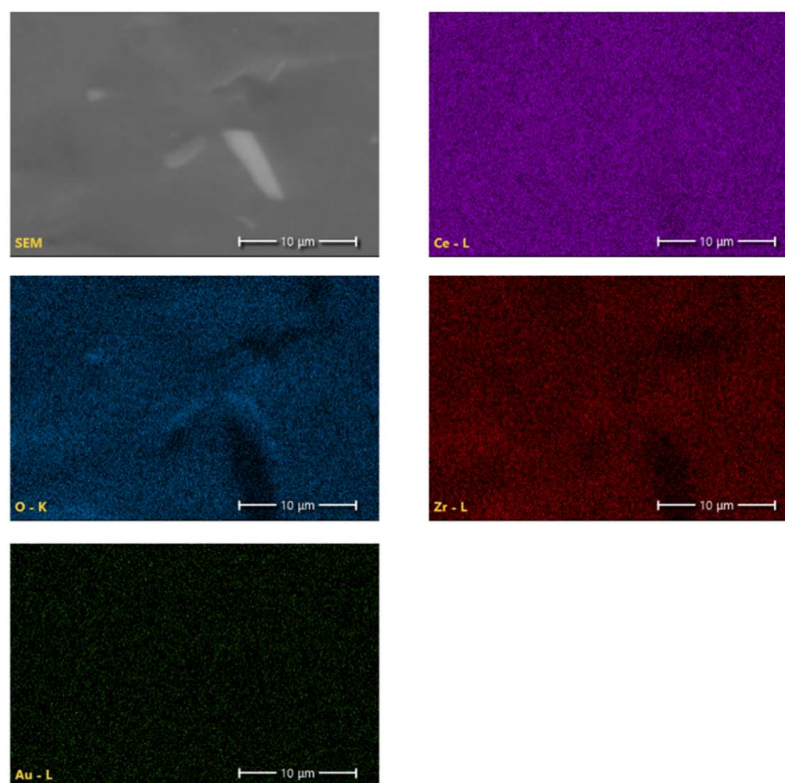


**Figure 8.** Elemental maps of cerium, oxygen, zirconium and gold in Au/Zr<sub>0.93</sub>Ce<sub>0.07</sub>O<sub>2</sub>.

### 3. Materials and Methods

#### 3.1. Support and Catalyst Synthesis

All of the zirconium-doped ceria supports and cerium-doped zirconium supports were obtained with two precursors, namely ammonium ceric nitrate (analytical grade, POCh Gliwice, Gliwice, Poland) and zirconyl nitrate (analytical grade, POCh Gliwice, Gliwice, Poland). Both compounds were dissolved in redistilled water, mixed and diluted before co-precipitation. Then, a sufficient amount of ammonia water (analytical grade, POCh Gliwice, Gliwice, Poland) was added while stirring. The formed precipitate was filtered off under reduced pressure using a vacuum water jet pump. It was thoroughly washed with redistilled water until the pH of the filtrate was neutral. The precipitate was dried in an evaporating dish and calcined for 4 h at 550 °C. The reference samples, namely CeO<sub>2</sub> and ZrO<sub>2</sub>, were obtained in accordance with the same procedure.

The catalysts were obtained by depositing gold onto the calcined supports using wet impregnation with solutions of  $\text{HAuCl}_4 \cdot \text{H}_2\text{O}$  (analytical grade, Sigma-Aldrich, St. Gallen, Switzerland). The solution had a concentration to give 1 wt.% of gold, which was based on previous experiments and assumed 80% efficiency. The pH of the solution was adjusted to approximately 8 with the appropriate amount of a concentrated  $\text{K}_2\text{CO}_3$  solution (POCh Gliwice, Gliwice, Poland). After deposition, the precipitate was washed with redistilled water until no chloride ions were present in the filtrate, dried and calcined at  $350\text{ }^\circ\text{C}$  for 3 h. Then, in order to obtain two different gold particle sizes, the support loaded with gold was divided into two parts and one of them was calcined at  $550\text{ }^\circ\text{C}$  for 3 h, whereas the other was kept at  $550\text{ }^\circ\text{C}$  for 7 h.

The silver catalysts were prepared with appropriate amounts of a  $\text{AgNO}_3$  solution (analytical grade, POCh Gliwice, Gliwice, Poland) dosed onto supports wetted with 1 mL of redistilled water. The  $\text{AgNO}_3$  solution was prepared using 0.23 g of the salt dissolved in 25 mL of redistilled water and 0.5 mL was used per 1 g of catalyst. After the solvent was evaporated, the solids were heated to  $200\text{ }^\circ\text{C}$  in order to decompose the nitrate and were then calcined for an hour at  $550\text{ }^\circ\text{C}$ .

Potassium carbonate (analytical grade, POCh Gliwice, Gliwice, Poland) was used to introduce potassium ions onto the surface of the catalysts using wet impregnation. The solution was prepared by dissolving 0.37 g of  $\text{K}_2\text{CO}_3$  in 50 mL of redistilled water. The appropriate volume of the solution was used to obtain the desired potassium ion loading and the catalyst was then dried. After drying, the catalysts were calcined for another hour at  $550\text{ }^\circ\text{C}$ .

### 3.2. Support and Catalyst Characterization

The secondary emission microscope imaging of the supports and catalysts were obtained using a Prisma E instrument (Field Electron and Ion Company, FEI, Hillsboro, OR, USA) with a working distance of 11 mm, spot size 3, beam energy 10 kV and beam deceleration of 5 kV. For each sample, images were collected at magnifications of 500, 1000, 2000, 5000, 10,000 and 20,000 times.

The specific surface areas of the supports and catalysts was determined with nitrogen physisorption using Micromeritics ASAP 2020 (Micromeritics Instrument Corp., Norcross, GA, USA). The measurements were performed at 77 K after 30 min of outgassing (0.5–1 g of sample) at  $150\text{ }^\circ\text{C}$  under vacuum. The specific surface area was calculated using the Brunauer–Emmett–Teller equation.

The X-ray photoelectron spectroscopy (XPS) was performed on a K-Alpha device (Thermo Scientific, Waltham, MA, USA). Survey spectra (200 eV, 1 eV/step) and the following detailed spectra (50 eV, 0.1 eV/step) were collected: C 1s (extended to 305 eV to include the K 2p doublet), O 1s, Ce 3d and Zr 3d, as well as Au 4f and Ag 3d. After a Shirley-type background subtraction, the spectra were calibrated to 285.0 eV for C 1s.

The X-ray diffraction studies were obtained in the range of  $20$  to  $140^\circ$  on a D5000 horizontal goniometer (Bruker AXS GmbH, Karlsruhe, Germany) using Cu  $\text{K}\alpha$  radiation ( $1.5418\text{ \AA}$ ), operating at 40 kV, 40 mA with divergent Bragg–Brentano beam optics. The LynxEye silicon strip detector was applied for data acquisition. The data were processed as described in [45]. The diffraction patterns in the manuscript are presented after subtracting the background, as they were fitted with an appropriate Voigt function. The Scherrer equation, Williamson–Hall plot, and extrapolation of the lattice constant by the Nelson–Riley function allowed us to calculate parameters such as: average particle size (of the support and of the active phase), cell parameters, microstrain parameter, etc. For the monoclinic phase, the lattice parameters were estimated by least squares fit to position of 10 reflexes but the data consistency and the obtained accuracy was markedly worse than for cubic lattice.

### 3.3. Activity Measurements

Activity measurements were carried out in a tubular one-piece glass reactor equipped with a condenser and a side arm for probing. In order to perform a test, 0.2 g of a catalyst was weighed out and placed into the aforementioned reactor. Next, 4.35 cm<sup>3</sup> of 2-pentanol (analytical grade, Sigma-Aldrich, St. Gallen, Switzerland; distilled prior to use) and 0.583 cm<sup>3</sup> of acetophenone (analytical grade, Sigma-Aldrich, St. Gallen, Switzerland; distilled prior to use) were added to the reactor and the reactor was placed in an oil bath preheated to 142–145 °C set on a hot plate with a magnetic stirrer. The oil temperature was measured using a thermocouple immersed directly in the oil bath. Samples were taken after 30 min and every hour for 6 hours from the beginning of the reaction. The composition of the samples was determined by a gas chromatograph (Agilent 6890N, Waldbronn, Germany) equipped with a WAX tracer capillary column.

## 4. Conclusions

The thorough investigation of the activity of monometallic gold and silver catalysts supported on zirconium-doped ceria (Ce<sub>1-x</sub>Zr<sub>x</sub>O<sub>2</sub>, where  $x < 0.2$ ) and cerium-doped zirconia (Zr<sub>1-x</sub>Ce<sub>x</sub>O<sub>2</sub>, where  $x < 0.1$ ) in catalytic transfer hydrogenation was performed. The results showed that:

- Large Au clusters (30 nm) were more active in catalytic transfer hydrogenation than small ones (4 nm).
- Heterogeneous silver catalysts supported on zirconium-doped ceria were highly active in catalytic transfer hydrogenation, whereas those on cerium-doped zirconia showed a much lower activity.
- Au and Ag supported on Ce<sub>1-x</sub>Zr<sub>x</sub>O<sub>2</sub>,  $x < 0.2$ , were much more active than on Zr<sub>1-x</sub>Ce<sub>x</sub>O<sub>2</sub>,  $x < 0.1$ .
- The effect of potassium ions depended on the loading:
  - The zirconium-doped ceria supports showed a positive effect of small doses of potassium ions on the activity in CTH, but negative effects of larger doses.
  - The presence of potassium ions on the activity of the most active gold and silver catalysts was negative, even at small loadings.
- Both types of supports contained only one phase: the Ce<sub>1-x</sub>Zr<sub>x</sub>O<sub>2</sub> supports had the fluorite-type structure, typical for undoped ceria and Zr<sub>1-x</sub>Ce<sub>x</sub>O<sub>2</sub> supports exhibited the structure of tetragonal zirconia. The activity of the former supports was strongly dependent on Zr loading, whereas that of the latter was not.

**Supplementary Materials:** The following is available online at <https://www.mdpi.com/article/10.3390/catal12090974/s1>, Figure S1: Assignment of reflexes of Ag/ZrO<sub>2</sub> to two zirconia polymorphs.

**Author Contributions:** Conceptualization, E.M.I.; formal analysis, E.M.I. and Z.K.; investigation, A.S., S.S., Z.K. and E.M.I.; resources, E.M.I. and M.G.; data curation, E.M.I. and Z.K.; writing—original draft preparation, E.M.I.; writing—review and editing, E.M.I.; visualization, E.M.I., S.S. and Z.K.; project administration, E.M.I.; methodology, E.M.I. and M.G.; funding acquisition, E.M.I. All authors have read and agreed to the published version of the manuscript.

**Funding:** This research was funded by the Scientific Discipline Board (RDN) for Chemical Engineering of the Warsaw University of Technology, grant number: 2022 I-CHEM.3-1.3.

**Acknowledgments:** We would also like to thank Peter Brodersen from the Ontario Centre for the Characterization of Advanced Materials (OCCAM) for the X-ray photoelectron spectroscopy measurements, and Donald W. Kirk for meaningful discussions regarding the research and manuscript.

**Conflicts of Interest:** The authors declare no conflict of interest.

## References

1. Anastas, P.T.; Warner, J.C. *Green Chemistry: Theory and Practice*; Oxford University Press: New York, NY, USA, 1998; p. 30.
2. Gliński, M. Catalytic hydrogen transfer over magnesia: Vapour and liquid phase reduction of various aralkyl ketones. *Appl. Catal. A Gen.* **2008**, *349*, 133–139. [[CrossRef](#)]
3. Mannu, A.; Grabulosa, A.; Baldino, S. Transfer Hydrogenation from 2-propanol to Acetophenone Catalyzed by [RuCl<sub>2</sub>(η<sup>6</sup>-arene)P] (P = monophosphine) and [Rh(PP)<sub>2</sub>]X (PP = diphosphine, X = Cl<sup>-</sup>, BF<sub>4</sub><sup>-</sup>) Complexes. *Catalysts* **2020**, *10*, 162. [[CrossRef](#)]
4. Vásquez, P.B.; Tabanelli, T.; Monti, E.; Albonetti, S.; Bonincontro, D.; Dimitratos, N.; Cavani, F. Gas-Phase Catalytic Transfer Hydrogenation of Methyl Levulinate with Ethanol over ZrO<sub>2</sub>. *ACS Sustain. Chem. Eng.* **2019**, *7*, 8317–8330. [[CrossRef](#)]
5. Alshammari, A.S. Heterogeneous Gold Catalysis: From Discovery to Applications. *Catalysts* **2019**, *9*, 402. [[CrossRef](#)]
6. Meyer, R.; Shaikhutdinov, S.K.; Freund, H.-J. Surface chemistry of catalysis by gold. *Gold Bull.* **2004**, *37*, 72–124. [[CrossRef](#)]
7. Calaza, F.; Mahapatra, M.; Neurock, M.; Tysse, W.T. Disentangling ensemble, electronic and coverage effects on alloy catalysts: Vinyl acetate synthesis on Au/Pd(1 1 1). *J. Catal.* **2014**, *312*, 37–45. [[CrossRef](#)]
8. Chen, M.; Kumar, D.; Yi, C.-W.; Goodman, D.W. The promotional effect of gold in catalysis by palladium–gold. *Science* **2005**, *310*, 291–293. [[CrossRef](#)]
9. Haruta, M.; Kobayashi, T.; Sano, H.; Yamada, N. Novel gold catalysts for the oxidation of carbon-monoxide at a temperature far below 0 °C. *Chem. Lett.* **1987**, *16*, 405–408. [[CrossRef](#)]
10. Solsona, B.E.; Garcia, T.; Jones, C.; Taylor, S.H.; Carley, A.F.; Hutchings, G.J. Supported gold catalysts for the total oxidation of alkanes and carbon monoxide. *Appl. Catal. A Gen.* **2006**, *312*, 67–76. [[CrossRef](#)]
11. Liotta, L.F.; Di Carlo, G.; Pantaleo, G.; Venezia, A.M. Supported gold catalysts for CO oxidation and preferential oxidation of CO in H<sub>2</sub> stream: Support effect. *Catal. Today* **2010**, *158*, 56–62. [[CrossRef](#)]
12. Nkosi, B.; Coville, N.J.; Hutchings, G.J. Reactivation of a supported gold catalyst for acetylene hydrochlorination. *J. Chem. Soc. Chem. Commun.* **1988**, 71–72. [[CrossRef](#)]
13. Scirè, S.; Liotta, L.F. Supported gold catalysts for the total oxidation of volatile organic compounds. *Appl. Catal. B Environ.* **2012**, *125*, 222–246. [[CrossRef](#)]
14. Prati, L.; Rossi, M. Gold on carbon as a new catalyst for selective liquid phase oxidation of diols. *J. Catal.* **1988**, *176*, 552–560. [[CrossRef](#)]
15. Flytzani-Stephanopoulos, M. Gold Atoms Stabilized on Various Supports Catalyze the Water-Gas Shift Reaction. *Acc. Chem. Res.* **2014**, *47*, 783–792. [[CrossRef](#)]
16. Claus, P.; Brückner, A.; Mohr, C.; Hofmeister, H. Supported Gold Nanoparticles from Quantum Dot to Mesoscopic Size Scale: Effect of Electronic and Structural Properties on Catalytic Hydrogenation of Conjugated Functional Groups. *J. Am. Chem. Soc.* **2000**, *122*, 11430–11439. [[CrossRef](#)]
17. Bond, G.C.; Sermon, P.A. Gold catalysts for olefin hydrogenation. *Gold Bull.* **1973**, *6*, 102–105. [[CrossRef](#)]
18. Silva, R.J.M.; Fiorio, J.L.; Vidinha, P.; Rossi, L.M. Gold Catalysis for Selective Hydrogenation of Aldehydes and Valorization of Bio-Based Chemical Building Blocks. *J. Braz. Chem. Soc.* **2019**, *30*, 2162–2169. [[CrossRef](#)]
19. Schimpf, S.; Lucas, M.; Mohr, C.; Rodemerck, U.; Brückner, A.; Radnik, J.; Hofmeister, C.P. Supported gold nanoparticles: In-depth catalyst characterization and application in hydrogenation and oxidation reactions. *Catal. Today* **2002**, *72*, 63–78. [[CrossRef](#)]
20. Wang, D.; Astruc, D. The Golden Age of Transfer Hydrogenation. *Chem. Rev.* **2015**, *115*, 6621–6686. [[CrossRef](#)]
21. Gorin, D.J.; Toste, F.D. Relativistic Effects in Homogeneous Gold Catalysis. *Nature* **2007**, *446*, 395–403. [[CrossRef](#)]
22. Zhang, M.; Yang, H.; Zhang, Y.; Zhu, C.; Li, W.; Cheng, Y.; Hu, H. Direct Reductive Amination of Aromatic Aldehydes Catalyzed by Gold(I) Complex under Transfer Hydrogenation Conditions. *Chem. Commun.* **2011**, *47*, 6605–6607. [[CrossRef](#)] [[PubMed](#)]
23. Fujita, T.; Guan, P.F.; McKenna, K.; Lang, X.Y.; Hirata, A.; Zhang, L.; Tokunaga, T.; Arai, S.; Yamamoto, Y.; Tanaka, N.; et al. Atomic Origins of the High Catalytic Activity of Nanoporous Gold. *Nat. Mater.* **2012**, *11*, 775–780. [[CrossRef](#)] [[PubMed](#)]
24. Su, F.-Z.; He, L.; Ni, J.; Cao, Y.; He, H.-Y.; Fan, K.-N. Efficient and chemoselective reduction of carbonyl compounds with supported gold catalysts under transfer hydrogenation conditions. *Chem. Commun.* **2008**, 3531–3533. [[CrossRef](#)] [[PubMed](#)]
25. Chiu, P.L.; Lee, H.M. Chemistry of the PCNHCP Ligand: Silver and Ruthenium Complexes, Facial/Meridional Coordination, and Catalytic Transfer Hydrogenation. *Organometallics* **2005**, *24*, 1692–1702. [[CrossRef](#)]
26. Liu, M.; Zhou, F.; Jia, Z.; Li, C.-J. A silver-catalyzed transfer hydrogenation of aldehyde in air and water. *Org. Chem. Front.* **2014**, *1*, 161–166. [[CrossRef](#)]
27. Wang, S.; Huang, H.; Tsareva, S.; Bruneau, C.; Fischmeister, C. Silver Catalyzed Hydrogenation of Ketones under Mild Conditions. *Adv. Synth. Catal.* **2019**, *361*, 786–790. [[CrossRef](#)]
28. Li, A.Y.; Kaushik, M.; Li, C.J.; Moores, A. Microwave-assisted synthesis of magnetic carboxymethyl cellulose-embedded Ag-Fe<sub>3</sub>O<sub>4</sub> nanocatalysts for selective carbonyl hydrogenation. *ACS Sustain. Chem. Eng.* **2016**, *4*, 965–973. [[CrossRef](#)]
29. Mertens, P.G.N.; Vandezande, P.; Ye, X.; Poelman, H.; Vankelekom, I.F.J.; De Vos, D.E. Recyclable Au<sup>0</sup>, Ag<sup>0</sup> and Au<sup>0</sup>-Ag<sup>0</sup> nanocolloids for the chemoselective of α,β-unsaturated aldehydes and ketones to allylic alcohols. *Appl. Catal. A Gen.* **2009**, *355*, 176–183. [[CrossRef](#)]
30. Claus, P.; Hofmeister, H. Electron Microscopy and Catalytic Study of Silver Catalysts: Structure Sensitivity of the Hydrogenation of Crotonaldehyde. *J. Phys. Chem. B* **1999**, *103*, 2766–2775. [[CrossRef](#)]
31. Deng, X.; Li, M.; Zhang, J.; Hu, X.; Zheng, J.; Zhang, N.; Chen, B.H. Constructing nano-structure on silver/ceria-zirconia towards highly active and stable catalyst for soot oxidation. *Chem. Eng. J.* **2017**, *313*, 544–555. [[CrossRef](#)]

32. Liens, A.; Reveron, H.; Douillard, T.; Blanchard, N.; Lughì, V.; Sergo, V.; Laquai, R.; Müller, B.R.; Bruno, G.; Schomer, S.; et al. Phase transformation induces plasticity with negligible damage in ceria-stabilized zirconia-based ceramics. *Acta Mater.* **2019**, *183*, 261–273. [[CrossRef](#)]
33. Tsukuma, K.; Shimada, M. Strength, fracture toughness and Vickers hardness of CeO<sub>2</sub>-stabilized tetragonal ZrO<sub>2</sub> polycrystals (Ce-TZP). *J. Mater. Sci.* **1985**, *20*, 1178–1184. [[CrossRef](#)]
34. El Attaoui, H.; Saâdaoui, M.; Chevalier, J.; Fantozzi, G. Static and cyclic crack propagation in Ce-TZP ceramics with different amounts of transformation toughening. *J. Eur. Ceram. Soc.* **2007**, *27*, 483–486. [[CrossRef](#)]
35. Querino, P.S.; Bispo, J.R.C.; Rangel, M.C. The effect of cerium on the properties of Pt/ZrO<sub>2</sub> catalysts in the WGS. *Catal. Today* **2005**, *107–108*, 920–925. [[CrossRef](#)]
36. Morozova, L.V.; Drozdova, I.A. Synthesis of Dispersed Mesoporous Powders of Solid Solution Zr<sub>0.88</sub>Ce<sub>0.12</sub>O<sub>2</sub> for Catalyst Carrier of the Conversion of Methane to Synthesis-Gas. *Inorg. Mater. Appl. Res.* **2020**, *11*, 1244–1252. [[CrossRef](#)]
37. Lu, H.-F.; Zhou, Y.; Han, W.-F.; Huang, H.-F.; Chen, Y.-F. High thermal stability of ceria-based mixed oxide catalysts supported on ZrO<sub>2</sub> for toluene combustion. *Catal. Sci. Technol.* **2013**, *3*, 1480. [[CrossRef](#)]
38. Sohn, J.R.; Lee, S.H.; Lim, J.S. New solid superacid catalyst prepared by doping ZrO<sub>2</sub> with Ce and modifying with sulfate and its catalytic activity for acid catalysis. *Catal. Today* **2006**, *116*, 143–150. [[CrossRef](#)]
39. Chen, L.; Li, J.; Ge, M. The poisoning effect of alkali metals doping over nano V<sub>2</sub>O<sub>5</sub>-WO<sub>3</sub>/TiO<sub>2</sub> catalysts on selective catalytic reduction of NO<sub>x</sub> by NH<sub>3</sub>. *Chem. Eng. J.* **2011**, *170*, 531–537. [[CrossRef](#)]
40. Haneda, M.; Kintaichi, Y.; Bion, N.; Hamada, H. Alkali metal-doped cobalt oxide catalysts for NO decomposition. *Appl. Catal. B Environ.* **2003**, *46*, 473–482. [[CrossRef](#)]
41. Pacultová, K.; Klegova, A.; Karásková, K.; Fridrichová, D.; Bílková, T.; Koštejn, M.; Obalová, L. Oxygen effect in NO direct decomposition over K/Co-Mg-Mn-Al mixed oxide catalyst—Temperature programmed desorption study. *J. Mol. Catal.* **2021**, *510*, 111695. [[CrossRef](#)]
42. Sun, H.; Qiu, P.; Yang, Y.; Liu, J.; Zhang, L.; Liu, Z. Molecular insights into the vinyl acetate synthesis on Pd/Au (111) Surface: Effects of potassium ion. *Appl. Surf. Sci.* **2022**, *571*, 151297. [[CrossRef](#)]
43. Parida, K.; Mishra, H.K. Catalytic ketonisation of acetic acid over modified zirconia. *J. Mol. Catal. A Chem.* **1999**, *139*, 73–80. [[CrossRef](#)]
44. Li, Y.; Zhang, C.; He, H.; Zhang, J.; Chen, M. Influence of alkali metals on Pd/TiO<sub>2</sub> catalysts for catalytic oxidation of formaldehyde at room temperature. *Catal. Sci. Technol.* **2016**, *6*, 2289–2295. [[CrossRef](#)]
45. Iwanek, E.; Liotta, L.F.; Williams, S.; Hu, L.; Calilung, L.F.; Pantaleo, G.; Kaszukur, Z.; Kirk, D.W.; Gliński, M. Application of Potassium Ion Deposition in Determining the Impact of Support Reducibility on Catalytic Activity of Au/Ceria-Zirconia Catalysts in CO Oxidation, NO Oxidation, and C<sub>3</sub>H<sub>8</sub> Combustion. *Catalysts* **2020**, *10*, 688. [[CrossRef](#)]
46. Iwanek, E.M.; Liotta, L.F.; Williams, S.; Hu, L.; Ju, H.; Pantaleo, G.; Thapar, A.; Kaszukur, Z.; Kirk, D.W.; Gliński, M. Activity of Ag/CeZrO<sub>2</sub>, Ag+K/CeZrO<sub>2</sub>, and Ag-Au+K/CeZrO<sub>2</sub> Systems for Lean Burn Exhaust Clean-Up. *Catalysts* **2021**, *11*, 1041. [[CrossRef](#)]
47. Iwanek (nee Wilczkowska), E.M.; Liotta, L.F.; Williams, S.; Hu, L.; Ju, H.; Pantaleo, G.; Kaszukur, Z.; Kirk, D.W.; Patkowski, W.; Gliński, M. Reducibility Studies of Ceria, Ce<sub>0.85</sub>Zr<sub>0.15</sub>O<sub>2</sub> (CZ) and Au/CZ Catalysts after Alkali Ion Doping: Impact on Activity in Oxidation of NO and CO. *Catalysts* **2022**, *12*, 524. [[CrossRef](#)]
48. Kowalik, P.; Próchniak, W.; Borowiecki, T. The effect of alkali metals doping on properties of Cu/ZnO/Al<sub>2</sub>O<sub>3</sub> catalyst for water gas shift. *Catal. Today* **2011**, *176*, 144–148. [[CrossRef](#)]
49. Shah, P.M.; Burnett, J.W.H.; Morgan, D.J.; Davies, T.E.; Taylor, S.H. Ceria–Zirconia Mixed Metal Oxides Prepared via Mechanochemical Grinding of Carbonates for the Total Oxidation of Propane and Naphthalene. *Catalysts* **2019**, *9*, 475. [[CrossRef](#)]